NANO · MICRO small
www.small-journal.com

Boosting Interleukin-12 Antitumor Activity and Synergism with Immunotherapy by Targeted Delivery with isoDGR-Tagged Nanogold

Anna Maria Gasparri, Angelina Sacchi, Veronica Basso, Filippo Cortesi, Massimo Freschi, Eltjona Rrapaj, Matteo Bellone, Giulia Casorati, Paolo Dellabona, Anna Mondino, Angelo Corti, and Flavio Curnis**

The clinical use of interleukin-12 (IL12), a cytokine endowed with potent immunotherapeutic anticancer activity, is limited by systemic toxicity. The hypothesis is addressed that gold nanoparticles tagged with a tumor-homing peptide containing isoDGR, an $\alpha v\beta 3$-integrin binding motif, can be exploited for delivering IL12 to tumors and improving its therapeutic index. To this aim, gold nanospheres are functionalized with the head-to-tail cyclized-peptide CGisoDGRG (Iso1) and murine IL12. The resulting nanodrug (Iso1/Au/IL12) is monodispersed, stable, and bifunctional in terms of $\alpha v\beta 3$ and IL12-receptor recognition. Low-dose Iso1/Au/IL12, equivalent to 18–75 pg of IL12, induces antitumor effects in murine models of fibrosarcomas and mammary adenocarcinomas, with no evidence of toxicity. Equivalent doses of Au/IL12 (a nanodrug lacking Iso1) fail to delay tumor growth, whereas 15 000 pg of free IL12 is necessary to achieve similar effects. Iso1/Au/IL12 significantly increases tumor infiltration by innate immune cells, such as NK and iNKT cells, monocytes, and neutrophils. NK cell depletion completely inhibits its antitumor effects. Low-dose Iso1/Au/IL12 can also increase the therapeutic efficacy of adoptive T-cell therapy in mice with autochthonous prostate cancer. These findings indicate that coupling IL12 to isoDGR-tagged nanogold is a valid strategy for enhancing its therapeutic index and sustaining adoptive T-cell therapy.

1. Introduction

Interleukin-12 (IL12) is a heterodimeric immunostimulatory cytokine showing anticancer and antimetastatic properties in several preclinical models.[1] This protein can stimulate the proliferation and cytotoxic functions of NK, NKT, and $CD8^+$ T cells,[2] induce the differentiation of naïve $CD4^+$ T cells into T helper type 1 (Th1) cells,[3] and promote the production of interferon-γ (IFNγ).[4] This cytokine, in turn, can act on tumor cells, macrophages, lymphocytes, and endothelial cells to favor cell-mediated immunity and to induce antiangiogenic effects,[5] IL12 can also directly act on dendritic cells to stimulate IL12 production and to enhance antigen presentation.[6]

Unfortunately, clinical studies in cancer patients showed that systemic administration of IL12 was accompanied by unacceptable systemic toxicity and, in few cases, even by fatal events,[7] which dramatically precluded its direct exploitation in cancer treatment.[1e,f]

To reduce the dose of IL12 necessary for inducing antitumor effects and, consequently, its systemic toxicity, various drug delivery systems have been developed so far. For example, peptides,[8] antibodies,[9] liposomes,[10] biopolymer,[11] polymeric nanoparticles, and nanogels have been used as vehicles for delivering IL12 to tumors.[12] One compound (called NHS-IL12), consisting of two molecules of IL12 fused to a tumor necrosis-targeting human antibody, is under investigation in Phase I clinical trials alone or in combination with

Dr. A. M. Gasparri, A. Sacchi, Dr. E. Rrapaj, Dr. F. Curnis
Division of Experimental Oncology
IRCCS San Raffaele Scientific Institute
Milan 20132, Italy
E-mail: curnis.flavio@hsr.it

The ORCID identification number(s) for the author(s) of this article can be found under https://doi.org/10.1002/smll.201903462.

DOI: 10.1002/smll.201903462

Dr. V. Basso, Dr. F. Cortesi, Dr. M. Bellone, Dr. G. Casorati, Dr. P. Dellabona, Dr. A. Mondino
Division of Immunology
Transplantation and Infectious Diseases
IRCCS San Raffaele Scientific Institute
Milan 20132, Italy

Dr. M. Freschi
Department of Pathology
IRCCS San Raffaele Scientific Institute
Milan 20132, Italy

Prof. A. Corti
Division of Experimental Oncology
IRCCS San Raffaele Scientific Institute
Vita-Salute San Raffaele
Milan 20132, Italy
E-mail: corti.angelo@hsr.it

immune checkpoint inhibitors (see ref. [13] and clinicaltrials.gov; NCT01417546 and NCT02994953). Other approaches that exploit this cytokine for cancer therapy are based on the use of IL12-encoding DNA and electroporation,[14] viral vectors encoding IL12 or genetically engineered lymphocytes.[15]

The results of these studies suggest that targeted delivery of IL12 to tumors might represent a valid strategy for enhancing its therapeutic index. Thus, studies aimed at developing delivering systems that enable administration of extremely low, yet pharmacologically active, doses of IL12 to tumors are of great experimental and clinical interest.

We have previously shown that peptides containing isoAsp-Gly-Arg (isoDGR), a motif that recognizes the $\alpha v\beta 3$ integrin overexpressed in tumor vessels and on different tumor cell types,[16] can be exploited as ligands for targeted delivery of various drugs and nanoparticles to tumors.[16b,17] In particular, we have identified a head-to-tail-cyclized hexapeptide, CGisoDGRG (called Iso1), which recognizes $\alpha v\beta 3$ with high selectivity and affinity, binds tumor vessels, and works as an efficient ligand for delivering fluorescent nanoparticles or radioactive compounds to tumors.[17,18] The Iso1 peptide, after chemical conjugation to human serum albumin, has been exploited for tagging gold nanoparticles loaded with tumor necrosis factor-alpha (TNF), a cytokine endowed with antitumor activity.[17,19] Interestingly, nontoxic doses of this nanodrug can induce anticancer effects in tumor-bearing mice, by virtue of an active targeting mechanism.[17,19]

Iso1-tagged gold nanoparticles might represent, therefore, efficient vehicles for delivering cytokines to tumors and, consequently, for improving their therapeutic index. To address this hypothesis, we have prepared Iso1-tagged gold nanospheres bearing IL12 (Iso1/Au/IL12) and analyzed their therapeutic efficacy and mechanism of action in murine models of fibrosarcoma, mammary adenocarcinoma and autochthonous prostate adenocarcinoma (TRAMP), the latter in combination with adoptive T-cell therapy. We show that this nanoformulation enables the delivery of extremely low doses of IL12 (in the picogram range) to tumors, with antitumor effects. Furthermore, we show that this approach can substantially increase the therapeutic index of this cytokine alone and in combination with adoptive immunotherapy.

2. Results

2.1. Preparation and Characterization of Iso1/Au/IL12 and Au/IL12 Nanoparticles

Iso1/Au/IL12 was prepared by incubating 25 nm gold nanospheres with mixtures of Iso1-HSA, a peptide–albumin conjugate, and murine IL12, followed by a metoxy-PEG-thiol solution. Optimization studies showed that optimal loading could be achieved with 120 μg of Iso1-HSA and 2.7 μg of IL12 per mL of gold solution, at pH 5.5 (see Figures S1 and S2, Supporting Information). A nanodrug lacking Iso1 was also prepared (Au/IL12).

UV–vis spectrophotometric analysis of both products showed single absorption peaks at 530 nm with similar width, indicating that both nanodrugs contained little, or no, aggregates (**Figure 1**a and **Table 1**). Accordingly, dynamic light scattering (DLS) analysis showed that these nanodrugs had an average diameter of about 40 nm, suggesting that they were monodispersed (Table 1), and showed similar zeta potential. Furthermore, transmission electron microscopy (TEM) showed that both nanodrugs were made of gold nanospheres with an average diameter of about 27 nm (Figure S3, Supporting Information). Thus, the two nanodrugs had very similar physicochemical properties.

To assess the presence of IL12 and Iso1-HSA on these nanodrugs, we then measured their capability to bind the anti-IL12 mAb C15.6 and the integrin $\alpha v\beta 3$, spotted onto nitrocellulose filters. As expected, both Iso1/Au/IL12 and Au/IL12 could recognize the anti-IL12 antibody, whereas only Iso1/Au/IL12 could bind the integrin (Figure 1b). No binding of nanodrugs was observed to a soluble TNF receptor 2 fusion protein (sTNF-R2), an irrelevant protein used as negative control (Figure 1b). Moreover, Iso1/Au/IL12, but not Au/IL12, could bind $\alpha v\beta 3$ adsorbed onto microtiter plates, as detected by the anti-IL12 mAb C17.8 (Figure 1c). IL12-ELISA assays based on the use of two antibodies against the p40 subunit of IL12 (mAb C15.6 and mAb C17.8) could detect 4–5 molecules of IL12 per nanoparticle of Iso1/Au/IL12 and 12–13 molecules per nanoparticle of Au/IL12 (**Table 2**). Similar results were obtained with a different ELISA that detects the IL12 heterodimer form (p70). Finally, PEG-ELISA showed that 2–4 molecules of PEG/nanoparticle were loaded (Table 2).

2.2. IL12 Bound to Gold Is Biologically Active

To assess whether IL12 bound to gold could preserve its biological activity, we measured the capability of each nanodrug to induce the release of IFNγ from murine splenocytes. In this bioassay the EC_{50} of free IL12 was 21.6 ± 5.1 pg mL^{-1}, corresponding to $(169 \pm 40) \times 10^6$ molecules mL^{-1} (Table 2 and Figure 1d). Interestingly, the EC_{50} of Iso1/Au/IL12 and Au/IL12 were $(3.43 \pm 0.64) \times 10^6$ and $(3.38 \pm 0.83) \times 10^6$ nanoparticles mL^{-1} (Table 1 and Figure 1d), respectively, suggesting that the potency of each nanoparticle was equivalent to that of about 50 molecules of free IL12. The apparent higher number of IL12 molecules/nanoparticle detected by the bioassay, compared to the immunoassay (Table 2), may reflect the presence of bioactive IL12 molecules on the gold surface that were not recognized by the antibodies. An alternative explanation is that IL12 bound to gold can engage and activate more efficiently IL12 receptors, because of multivalent interactions.

2.3. IL12 and Iso1-HSA Are Stably Bound to Nanogold

The stability of protein–gold interactions in Iso1/Au/IL12 was then investigated. To this aim the presence of free IL12 in Iso1/Au/IL12 was first analyzed by IL12-ELISA after nanoparticle removal by centrifugation. IL12-ELISA of the supernatant showed the presence of 25 ng mL^{-1} IL12, corresponding to 0.9% of the total IL12 used for nanodrug preparation. Notably, no significant changes occurred upon nanodrug storage for 96 h at 4 °C or 140 d at –80 °C (Figure 1e). These results suggest that IL12 was firmly bound to gold and that no significant detachment occurred during drug storage. Furthermore, the

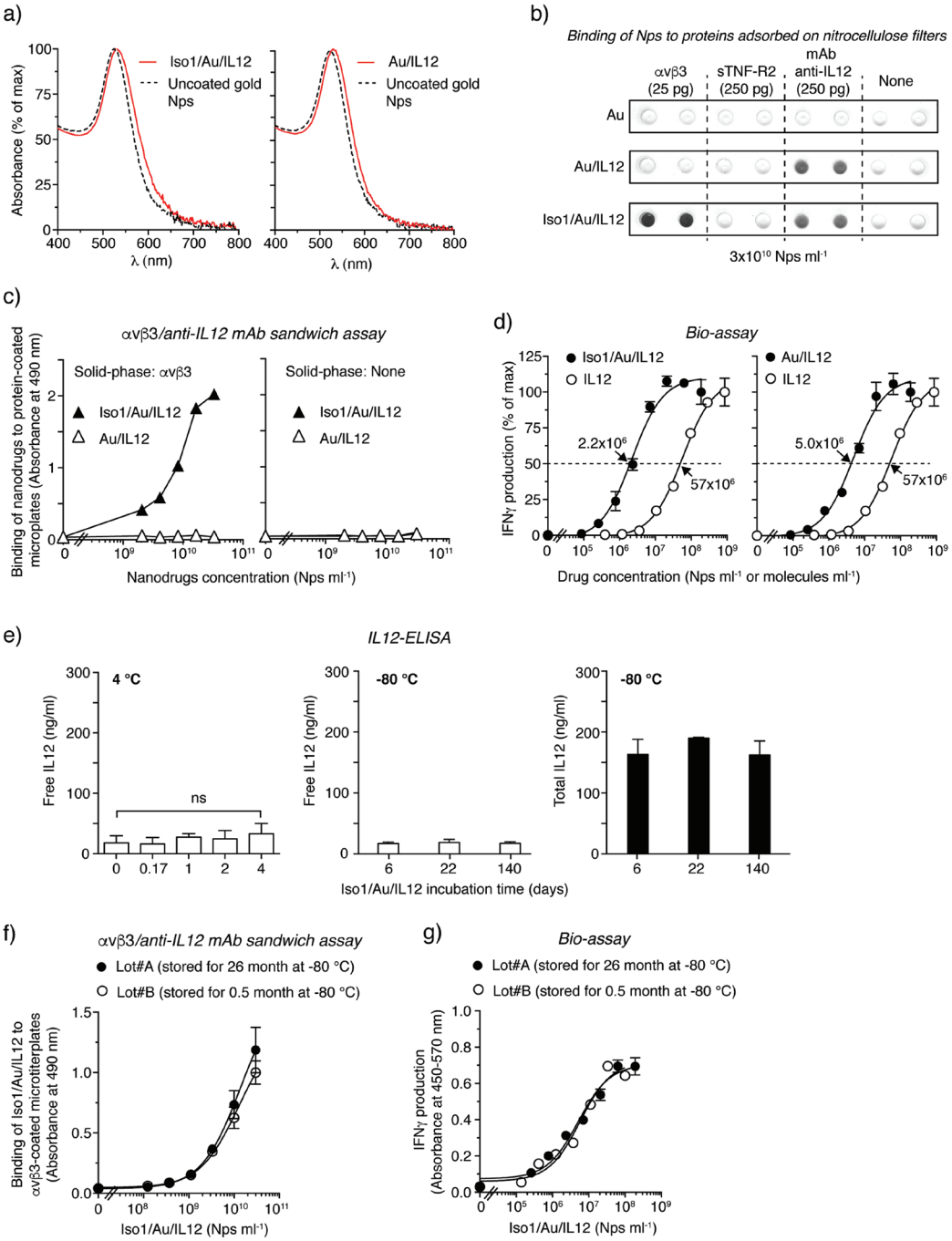

Figure 1. Characterization of Iso1/Au/IL12 and Au/IL12 nanodrugs. a) UV–vis absorption spectra of nanodrugs. Dotted line corresponds to uncoated 25 nm gold nanoparticles. b) Binding of nanodrugs to $\alpha v\beta 3$ receptor, soluble TNF receptor-2 (sTNF-R2), and anti-IL12 antibody (mAb C15.6) spotted onto nitrocellulose filters, as detected by silver staining of gold nanoparticles. The amount of each receptor spotted onto filters is indicated. sTNF-R2 was used as negative control. c) Binding of nanodrugs to $\alpha v\beta 3$ adsorbed onto microtiter plates, as detected with a biotinylated antibody IL12 (mAb C17.8) and HRP-labeled streptavidin. A representative experiment is shown. d) IFNγ production by murine splenocytes cultured with various amounts of nanodrugs or IL12. Murine splenocytes were cultured in vitro with complete medium supplemented with 125 U mL^{-1} of IL2 and the indicated amounts of gold nanoparticles or IL12 molecules (in quadruplicates) for 5 d. IFNγ production in pooled cell culture supernatants was determined by ELISA. One representative experiment is shown (mean±SE, two wells for each condition). e) Quantification of free IL12 (i.e., not bound to nanoparticles) (left and middle panels) and total IL12 (bound and free) (right panel) in Iso1/Au/IL12 after incubation at 4 °C or –80 °C for the indicated times. Total and free IL12 were detected by IL12-ELISA before and after centrifugation at 14 000 × g for 10 min, respectively. No significant release of IL12 occurred over the indicated times. f) Binding curves of Iso1/Au/IL12 (two different lots, #A and #B, stored for 0.5 or 26 months at –80 °C) to microtiter plated coated with $\alpha v\beta 3$. The two binding curves, detected with a biotinylated antibody against the IL12 (mAb C17.8) followed by HRP-labeled streptavidin, are similar. g) Production of IFNγ by murine splenocytes induced by different amounts of Iso1/Au/IL12 (Lot #A and Lot #B stored for 0.5 or 26 months at –80 °C), showing similar biological activities.

Table 1. Characterization of IL12-based nanodrugs and uncoated gold nanoparticles (Au) by UV–vis spectroscopy (UV–vis), dynamic light scattering (DLS), and zeta potential.

Nanodrugs or gold nanoparticles[a]	UV–vis[b]			DLS[c] radius [nm]	Zeta-potential[d] [mV]
	λ_{max} [nm]	PW 75%	650 nm/530 nm		
Iso1/Au/IL12 (pH 5.5)	528.6 ± 0.6	54.0 ± 3.5	0.104 ± 0.03	21.9 ± 3.2	−11.7 ± 1.1
Au/IL12 (pH 6.5)	528	57	0.071	17.9 ± 2.3	−11.2 ± 1.2
Uncoated Au	524.5 ± 0.6	52.0 ± 4.0	0.065 ± 0.02	11.56 ± 1.4	−28.3 ± 2.0

[a]Nanodrugs were prepared by mixing a mixture of Iso1-HSA and IL12 (120 µg: 2.7 µg, ratio) with 1 mL of gold ($A_{520\ nm}$: ≈1.0 optical density, with pH adjusted to the indicated value) See Experimental Sections; [b]λ_{max}: wavelength of peak absorbance; PW 75%: peak-width at 75% of height; 650 nm/530 nm: absorbance ratio. Mean±SD of two different preparations; [c]Mean±SD of two different preparations; [d]Mean±SD of three consecutive measurements.

$\alpha v\beta 3$ binding properties and the biological activity of Iso1/Au/IL12 freshly prepared or stored for 2 years at –80 °C were similar (Figure 1f,g). These and the above results, overall, suggest that the preparation of nanodrugs bearing functional IL12 and Iso1 is feasible and that the final product is stable.

2.4. Antitumor Activity of IL12-Based Nanodrugs in Murine Fibrosarcomas and Mammary Adenocarcinomas

The in vivo antitumor properties of Iso1/Au/IL12, Au/IL12 and IL12 were then investigated. Mice bearing established WEHI-164 fibrosarcomas were treated i.v. once a week with various doses of IL12, ranging from 4.7 to 15 000 pg, or with equivalent doses of nanodrugs (in terms of immunoreactive IL12 quantified by ELISA). Administration of 15 000 pg of IL12, but not of lower doses, induced significant delay of tumor growth (**Figure 2**a). Comparable antitumor effects were obtained with 19–75 pg of Iso1/Au/IL12 (Figure 2b), indicating that the nanodrug was about 200–800-fold more active than IL12. Notably, Au/IL12 (26 or 127 pg) was almost inactive, compared to Iso1/Au/IL12 (Figure 2c), pointing to isoDGR-mediated "*active*" targeting as a primary mechanism of accumulation of Iso1/Au/IL12 in tumors. Finally, higher doses of Iso1/Au/IL12 induced lower effects (Figure 2b), denoting a biphasic dose-response curve.

Both IL12 (15 000 pg) and Iso1/Au/IL12 (75 pg) significantly prolonged animal survival (Figure 2d). Of note, 2 out of 12 mice treated with Iso1/Au/IL12 were completely cured, whereas none was cured with IL12 at any tested dose.

No evidence of toxicity was observed at any of the tested doses and drugs, as judged from the lack of animal weight loss, lethargy, or ruffled fur (Figure S4A, Supporting Information and data not shown). When measuring drug stability, we found that similar antitumor effects were obtained with a batch of Iso1/Au/IL12 stored for 30 months at –80 °C (Figure S5, Supporting Information), indicating that this nanodrug was stable over time.

The antitumor activities of Iso1/Au/IL12 and IL12 were then investigated in the poorly immunogenic, aggressive TS/A mammary adenocarcinoma model. IL12 (70 or 350 pg) was completely inactive, even when the treatment was repeated for 5 consecutive days (**Figure 3**a). In contrast, 70 pg of Iso1/Au/IL12, significantly delayed the progression of established tumors (Figure 3b, upper panels). Similar results were obtained when the treatment was repeated twice per week (Figure 3b, lower panels). Also 350 pg of Iso1/Au/IL12 delayed tumor growth, although in this case the effect did not reach statistical significance. The finding that 350 pg of Iso1/Au/IL12 was less efficacious than the 70 pg dose supports the concept that the dose-response curve of this drug is biphasic, possibly because of activation of counter-regulatory mechanisms above a certain dose. Consistently, no significant antitumor effects were observed when Iso1/Au/IL12 (70 pg) was administered for five consecutive days (Figure 3b). Of note, two mice were cured in the groups treated once a week with 70 or 350 pg (none in the IL12 groups) and remained tumor-free after a rechallenge with a tumorigenic dose of TS/A cells to the end of the experiment (day 50). Also in this tumor model, no evidence of toxicity was obtained (Figure S4b, Supporting Information).

Overall, these results indicate that IL12 is endowed with markedly more potent antitumor activity when loaded on Iso1-tagged gold nanoparticles, compared to free IL12, owing to an isoDGR-mediated targeting mechanism.

Table 2. Quantification of IL12 and PEG molecules loaded on gold nanoparticles in Iso1/Au/IL12 and Au/IL12.

Nanodrugs or protein[a]	IL12			PEG[e]
	ELISA[b] [immunoreactive molecules/Np]	Bioassay[b] [bioactive molecules/Np]	Bioassay EC_{50}[d] [Np or IL12 molecules per mL]	ELISA [molecules/Np]
Iso1/Au/IL12 (pH 5.5)	4.5 ± 0.3 (n = 2)[c]	49 ± 9 (n = 6)	3.43 (±0.64) × 10^6 (n = 6)	3–4
Au/IL12 (pH 6.5)	12.4 ± 1.7 (n = 2)	44 ± 9 (n = 6)	3.80 (±0.83) × 10^6 (n = 5)	2–3
IL12	NA[f]	NA	169 (±40) × 10^6 (n = 12)	NA

[a]Nanodrugs were prepared by mixing a mixture of Iso1-HSA and IL12 (120 µg: 2.7 µg, ratio) with 1 mL of gold (A_{520} nm: ≈1.0 optical density, with pH adjusted to the indicated value). See Experimental Section; [b]Number of IL12 molecule bound to nanoparticles as determined by IL12-ELISA (p40-ELISA Kit) or by a biological assay based on the quantification of IFNγ secretion by murine splenocytes, using IL12 as reference standard. Mean±SE; [c]n, number of independent experiments, each in duplicate; [d]EC_{50} (effective concentration 50) of nanodrugs or IL12 was determined by measuring their effect on IFNγ secretion by murine splenocytes, using IL12 as reference standard. Mean±SE; [e]Number of mPEG molecules (mPEG-SH; 20 KDa) per nanoparticles, as determined by PEG-ELISA; [f]NA, not applicable.

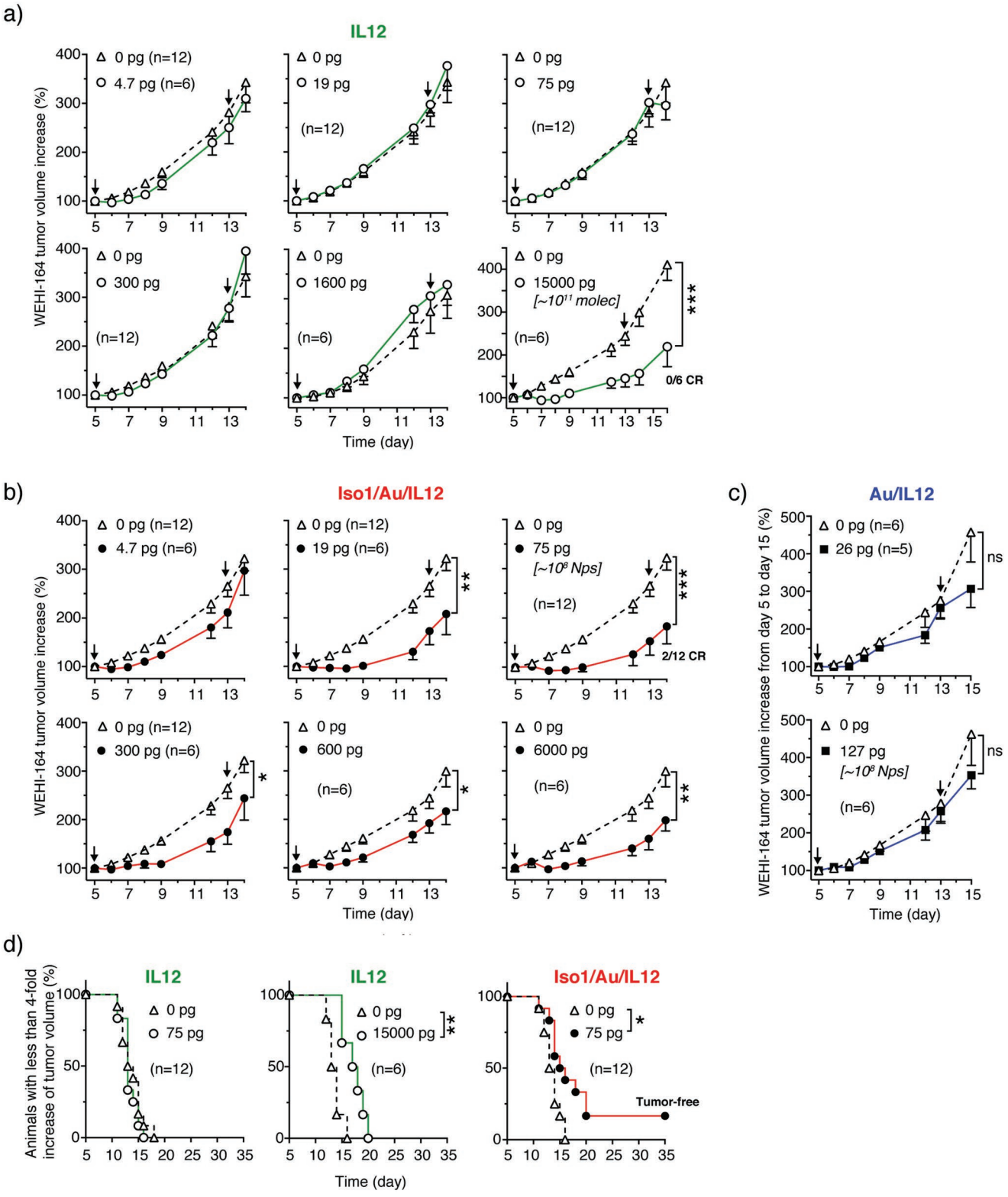

Figure 2. Antitumor effects of IL12, Iso1/Au/IL12, or Au/IL12, in the WEHI-164 fibrosarcoma model. a–c) Effect of IL12 or nanodrugs on tumor growth. Mice were treated at the indicated times after tumor implantation (arrows) with various doses of nanodrugs or IL12 (i.v.). All the indicated doses correspond to immunoreactive IL12, as detected by ELISA. Tumor volume increases are shown (mean ± SE). Numbers in parenthesis indicate the number of mice per dose (cumulative results of 1–2 independent experiments, six mice per experiment). *, $P < 0.05$; **, $P < 0.01$; ***, $P < 0.001$, by Mann–Whitney analysis of the area under the curve for each tumor, with the GraphPad Prism software (ns, not significant; CR, complete response). d) Kaplan-Maier curves of experimental group depicted in panels a and b. *, $P < 0.05$; **$P < 0.01$ by Log-rank (Mantel-Cox) test.

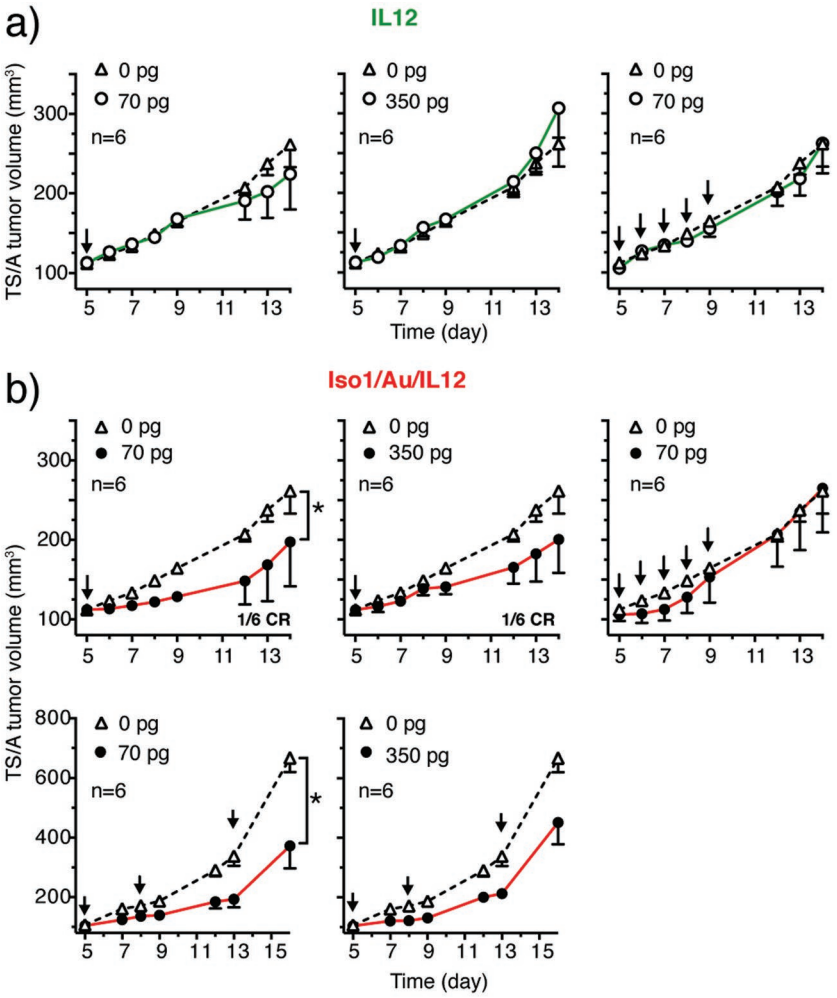

Figure 3. Antitumor effects of IL12 and Iso1/Au/IL12 in the TS/A adenocarcinoma model. Effect of a) IL12 or b) Iso1/Au/IL12 on tumor growth. Mice were treated at indicated times after tumor implantation (arrows) with the indicated doses of IL12 or Iso1/Au/IL12 (i.v.). All the indicated doses correspond to immunoreactive IL12, as detected by ELISA. Tumor volumes are shown (mean±SE, six mice per experiment). CR, complete response and tumor free at day 50 after a second challenge at day 32. *, $P < 0.05$, by Mann–Whitney analysis of the area under the curve for each tumor, with the GraphPad Prism software (CR, complete response).

2.5. Iso1/Au/IL12 Increases the Levels of sTNF-R2, IFNγ and MIP-2 in Tumor Microenvironment

To test the hypothesis that low-dose Iso1/Au/IL12 exerts local effects in tumors and little or no effects at the systemic level, we measured the amount of IFNγ, soluble TNF-R2 (sTNF-R2) and macrophage-inflammatory protein 2 (MIP-2) in tumors and in blood samples of mice bearing WEHI-164 tumors after treatment with Iso1/Au/IL12 (70 pg, administered i.v. at day 14, Figure S6, Supporting Information). These factors were chosen as representative of IL12-mediated effects.[4b,7b,20] Iso1/Au/IL12 significantly increased the levels of sTNF-R2 in tumors, but not in serum, 18 h later (Figure S6b, Supporting Information). This treatment could also increase the levels of IFNγ and MIP-2 in tumors, although in a non-significant manner, but not at all in serum (Figure S6c,d, Supporting Information). These results support the concept that low dose Iso1/Au/IL12 can affect the tumor microenvironment with minimal effects at the systemic level.

2.6. Iso1/Au/IL12 Increases the Infiltration of Innate Immune Cells in Fibrosarcomas

To investigate the antitumor effects of the Iso1/Au/IL12 at the cellular level, we then assessed the immune landscape of the tumor microenvironment by unsupervised flow cytometry analysis.[21] To this aim, we employed a panel of 14 mAbs to detect markers that distinguish innate and adaptive immune cells infiltrating the tumor microenvironment of fibrosarcoma-bearing mice, one week after the treatment with Iso1/Au/IL12 (18 pg) or vehicle. As expected, the treatment significantly reduced the tumor mass (Figure S7a, Supporting Information). The plotted viSNE map showed 51 clusters automatically defined by X-Shift algorithm,[22] five of which appeared differentially distributed between treated and untreated tumors (**Figure 4**a). To determine whether cell populations were actually changing in mice treated with Iso1/Au/IL12, compared to those treated with the vehicle, we extracted the frequency of single clusters in each sample. Out of the five differentially distributed clusters, three showed statistical significance (Figure 4b). To identify the cell population separated by X-Shift, we analytically compared all stained markers within each cluster (Figure 4c). The results showed that the clusters had the following phenotypes: Cluster 1: $CD11b^+$, $NKp46^+$, $CD3^-$ and $Ly6C^+$ (NK cells); Cluster 2: $CD11b^+$, $Ly6C^+$ $Ly6G^-$, $F4/80^{low}$ (inflammatory monocytes); Cluster 3: $CD11b^+$, $Ly6C^+$, $Ly6G^+$, $F4/80^-$ (neutrophils); Cluster 4: $CD3^+$, $CD4^+$ (T cells); Cluster 5: $CD19^+$ (B cells) (Figure 4c). Cluster 1 included also a small $CD3^+$ T population that was identified as invariant Natural Killer T (iNKT) cells by specific staining with PBS-57-loaded CD1d-tetramers (Figure 4d, upper panel). These cells increased significantly in Iso1/Au/IL12 treated mice (Figure 4d, lower panel). Analytical flow cytometry analyses confirmed that $CD11b^+$ cells, granulocytes, monocytes, and NK cells were significantly increased in tumor treated with Iso1/Au/IL12 (Figure 4e and Figure S7b, Supporting Information).

Remarkably, the antitumor activity of Iso1/Au/IL12 was completely inhibited by anti-asialo GM1 antibodies (**Figure 5**), a reagent antibody capable of depleting NK cells.[23]

These results, overall, suggest that low-dose Iso1/Au/IL12 is sufficient to modulate the tumor microenvironment favoring tumor infiltration by innate immune effectors, among which NK cells are found and shown to be critical for Iso1/Au/IL12 therapeutic effects.

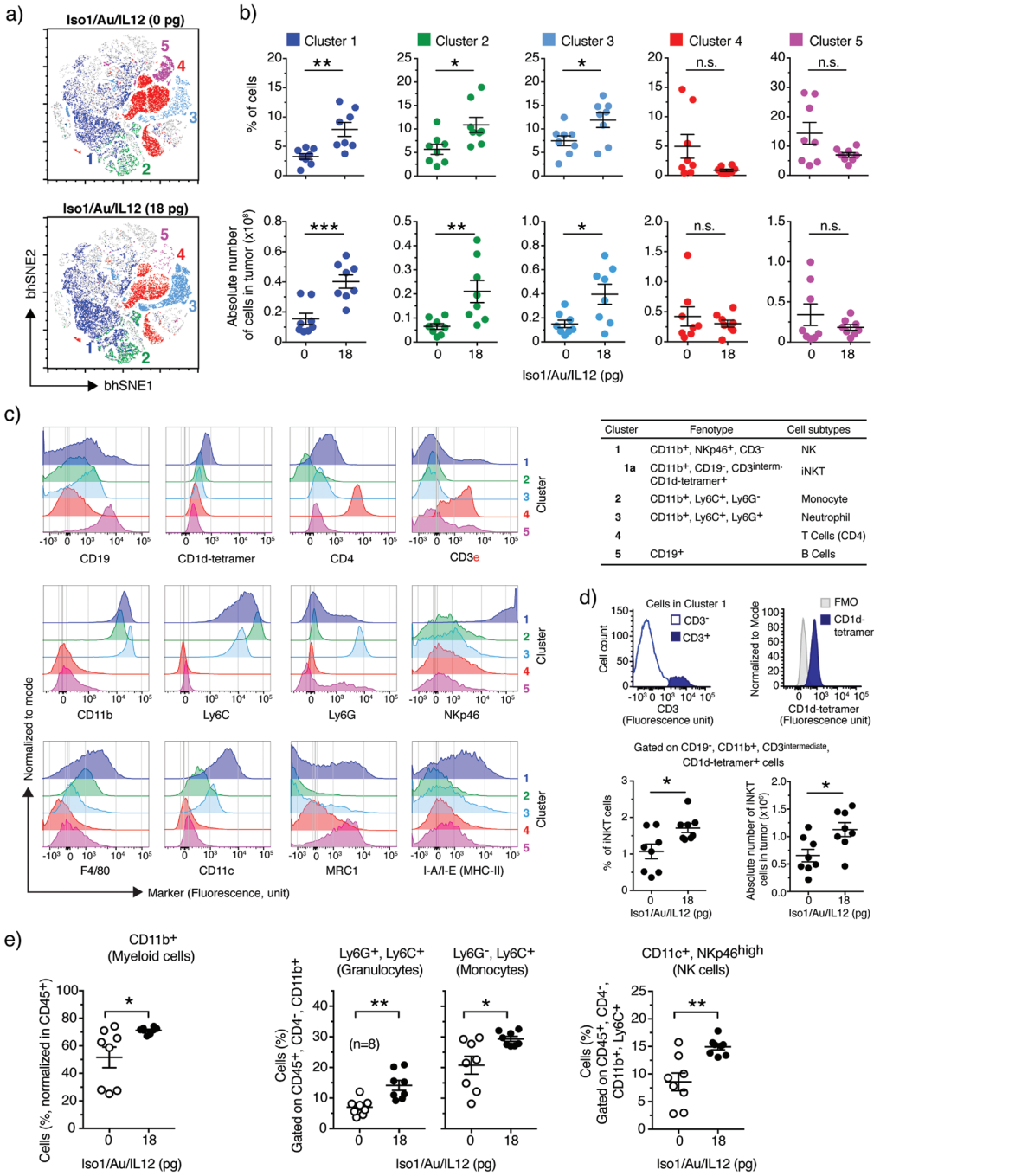

Figure 4. Effect of Iso1/Au/IL12 on immune cells infiltrating WEHI-164 tumors. WEHI-164 tumor-bearing animals were treated at day 6 after tumor implantation with 18 pg of Iso1/Au/IL12 or with diluent. On day 13 tumors were excised, processed to obtain a single cells suspension, and characterized for the expression of 14 identity markers by flow cytometry (see Experimental Section). a) High-dimensional bhSNE maps of tumor-infiltrating immune cells in untreated (upper) and Iso1/Au/IL12 treated mice (lower). Representative maps of the clusters identified by X-Shift algorithm (indicated as 1, 2, 3, 4, and 5 and color code) are shown. The shown maps result from the overlapping of four independent mice per condition. Shown are maps from one out of two independent experiments (giving comparable results). b) Quantification of percentage of cells (upper) and absolute cell numbers per tumor (lower) in Clusters 1, 2, 3, 4, and 5. Dots represent single mice. Mean±SE is shown. *, $P < 0.05$, **, $P < 0.01$, ***$P < 0.001$, by two-tailed t test. c) Expression of markers in cluster 1, 2, 3, 4 and 5 (right), and their corresponding specific phenotypes and cell subtypes (shown in the Table). d) Characterization of CD3 negative (empty square) and positive (filled square) cells within cluster 1. $CD3^+$ cells were identified as iNKT cells by reactivity to PBS-57-loaded CD1d-tetramer, as shown in the consecutive histogram. These cells are defined as cluster 1a (see Table in panel c). iNKT cells were then analytically gated and quantified as described in the above graphs. e) Quantification of $CD11b^+$ cells, granulocytes, monocytes, and NK cells in untreated and Iso1/Au/IL12 treated mice determined by analytical flow cytometry (see also Figure S7B, Supporting Information). Each dot represents a single mouse. Mean±SE is shown. *, $P < 0.05$, **, $P < 0.01$, by two-tailed t test. All frequencies are calculated on viable $CD45^+$ cells. b,d,e) Data show cumulative results of two independent experiments, each performed with four mice per group.

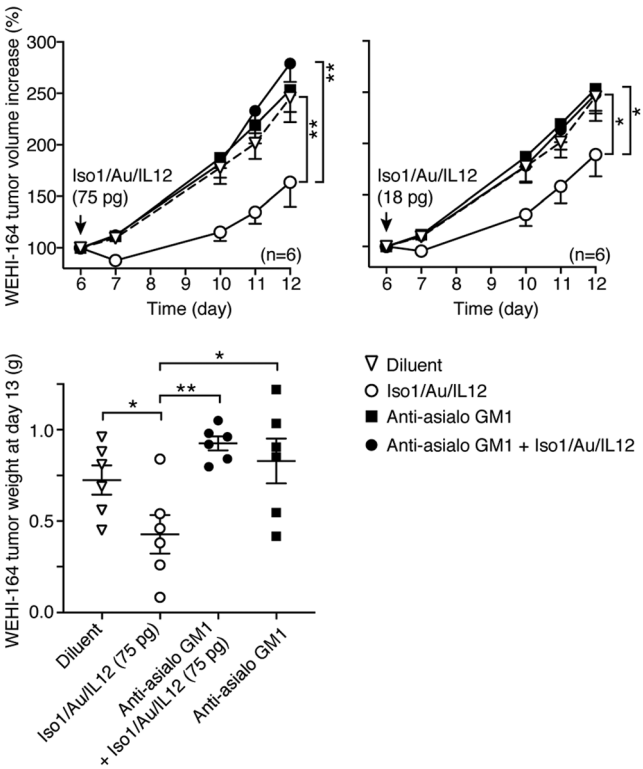

Figure 5. Effect of anti-asialo GM1 antibodies on the antitumor activity of Iso1/Au/IL12. WEHI-164 tumor-bearing mice (six mice per group) were injected with 40 µL of anti-asialo GM1 rabbit antibodies at day 3 and 5 and with the indicated doses of Iso1/Au/IL12 at day 6. The indicated doses correspond to immunoreactive IL12, as detected by ELISA. Tumor volumes and weights at the indicated times (mean±SE) are shown. *, $P < 0.05$; **, $P < 0.01$, by Mann–Whitney analysis of the area under the curve for each tumor volume or by two-tailed t test for tumor weights, with the GraphPad Prism software.

2.7. Iso1/Au/IL12 Increases the Efficacy of Adoptive T-Cell Therapy in Mice with Autochthonous Prostate cancer

Previous studies have shown that adoptive transfer of tumor-specific T cells engineered to express IL12 constitutively improved antitumor protection, which was, however, in some cases accompanied by lethal toxicity.[15b–e] Although more recent studies showed that toxicity could be limited by engineering T cells with inducible IL12 constructs,[15f] we reasoned that the controlled delivery of an extremely low-dose, well-defined, of IL12 might prove a safer approach. To test the hypothesis that low-dose Iso1/Au/IL12 might be of help in the context of adoptive T-cell therapy (ACT) we used the transgenic prostate adenocarcinoma mouse model (TRAMP), with autochthonous prostate cancer development, and T cells redirected by TCR gene transfer to the tumor-associated large T antigen.[24] Notably, previous studies have shown that in this model tumor-redirected T cells lack significant therapeutic activity, unless used in combination of vessel-targeted TNF or minor histocompatibility redirected T cells.[24] Twenty-week-old TRAMP mice, a time at which all mice have established adenocarcinomas,[24] were subjected to nonmyeloablative total body irradiation, to favor T cell engraftment, and then injected with T cells redirected against the tumor-associated SV40 large T antigen. One day later mice were treated i.v. with Iso1/Au/IL12 (18 pg) and, after 4 weeks, sacrificed to assess the tumor burden by histopathological analysis (see **Figure 6**a for the experimental scheme). Iso1/Au/IL12 or ACT did not induce significant antitumor effects when injected alone, while elicited significant tumor regression when combined (Figure 6b). Flow cytometry analysis of tumor draining lymph nodes, spleen and blood, indicated that, although similar frequency of adoptively transferred CD45.1$^+$ CD8$^+$ cells were observed in treated and control mice (Figure 6c), mice receiving ACT and Iso1/Au/IL12 had higher frequencies of TCR redirected tumor-specific T cells (identified as Vβ9$^+$ cells) in tumor-draining lymph nodes (TdLN), compared to controls (Figure 6d). Iso1/Au/IL12 treatment increased also the effector functions of the transferred tumor-specific T cells, as defined by their ability to express IFNγ in TdLN (Figure 6e), or granzyme B cells in blood and spleen (Figure 6f). Collectively, these results show that Iso1/Au/IL12 promotes the antitumor efficacy of ACT.

3. Discussion

This work demonstrates that the therapeutic index of IL12 can be substantially increased by a targeting approach based on the use of isoDGR-tagged gold nanospheres as a vehicle. In particular, targeted delivery of IL12 to tumors was achieved by coupling this cytokine to 25 nm nanogold tagged with Iso1-HSA, a peptide–protein conjugate previously shown to bind $\alpha v\beta 3$ with good affinity and to home to tumor vessels.[17] The choice of nanogold as a carrier was based on the fact that this nanomaterial has been used with other cytokines in patients and proven to be safe and stable.[25]

Studies on the physical, biochemical, and biological properties of this nanodrug (called Iso1/Au/IL12) showed that the final product was monodispersed and that it could bind anti-IL12 antibodies and $\alpha v\beta 3$, as expected. The results also show that about 4 molecules of immunoreactive IL12 were present on the surface of each nanoparticle, as measured by IL12-ELISA. However, the biological potency of each nanoparticle was equivalent to that of 50 molecules of IL12, as measured by a bioassay based on murine splenocytes. Possibly, IL12 bound to the nanogold surface has a lower immunoreactivity or engages IL12 receptors on splenocytes more efficiently, compared to free IL12. Although these possibilities are not mutually exclusive, we favor the second hypothesis, considering that the total bioactive IL12 detected in the nanodrug was two-threefold greater than the total bioactive IL12 used for nanodrug preparation. More efficient engagement of IL12 receptors might be due to multivalent high avidity interactions between nanoparticles and cells.

Drug stability studies showed that Iso1/Au/IL12 can be stored for up to 2.5 years at –80 °C without loss of biological properties, both in terms of binding to $\alpha v\beta 3$ and IL12 receptors and of antitumor activity. Thus, adsorption of Iso1-HSA and IL12 on the nanogold surface is a valuable strategy for the preparation of stable and bifunctional conjugates endowed of both targeting (isoDGR) and effector (IL12) activity.

The results of in vivo studies performed in mice bearing subcutaneous WEHI-164 fibrosarcomas and TS/A adenocarcinomas

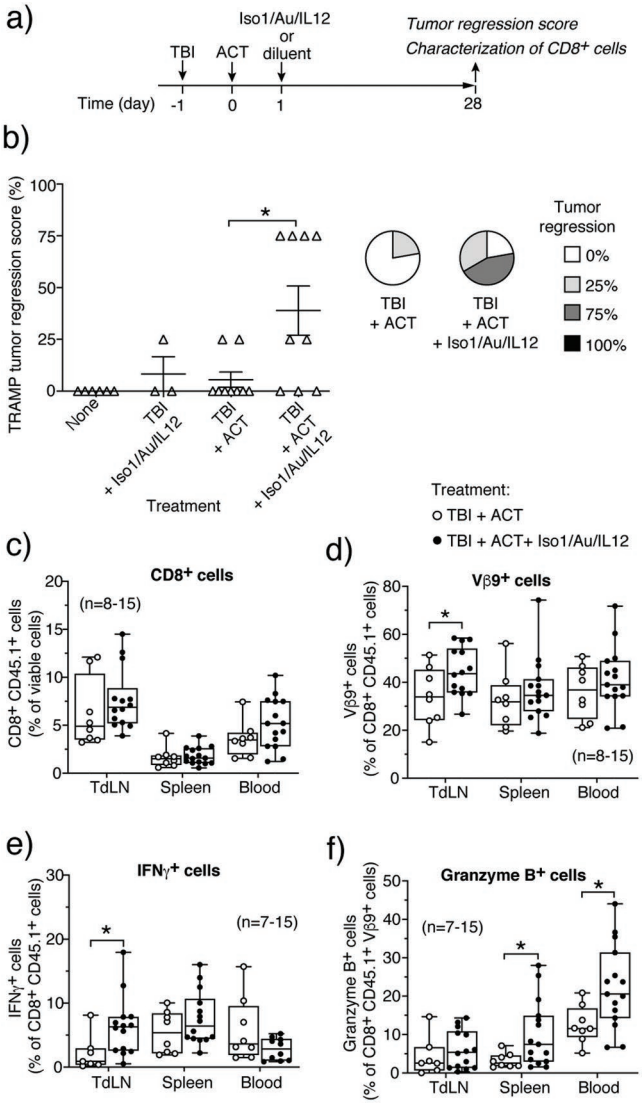

Figure 6. Effect of Iso1/Au/IL12 in combination with adoptive T cell therapy (ACT) in mice with autochthonous prostate cancer (TRAMP model). a) Experimental scheme. 20 week old TRAMP mice received total body irradiation (TBI) at day-1, the following day they received an i.v. injection of T cells redirected to the large T antigen (ACT). One day later, mice were treated without (ACT) or with Iso1/Au/IL12 (18 pg; ACT+ Iso1/Au/IL12). After 4 weeks, mice were sacrificed to determine the state of tumor growth by histopathological examination of the prostate and quantify tumor-directed T cell responses in tumor draining lymph nodes (TdLN), spleen and blood were processed and analyzed by flow cytometry. b) Effect of treatments on tumor growth. Coded H&E prostate tissue sections were scored as follows: complete regression (100%), defined as area without evidence of residual diseases; partial regression (25–75%), defined as area of complete regression scattered among acini affected by adenocarcinoma or no regression (0%). Triangles represent individual mice. Mean±SE is shown. *, $P < 0.05$ by $\chi 2$ test. The pie graphs summarize the fraction of mice in each group, according to the tumor regression score. c–f) Characterization of $CD8^+$ cells in TdLN, spleen, and blood from mice treated as indicated in panel A. c) Frequency of $CD8^+CD45.1^+$ viable cells. d) Frequencies of $V\beta9^+$ cells TCR redirected tumor-specific T cells. e) Frequency of tumor-specific T cells capable to produce IFNγ. f) Frequency of $V\beta9^+$ tumor-specific T cells with cytotoxic activity (identified as granzyme B+ cells). Cumulative results of two to three independent experiments. Box-plots with median, interquartile and 5–95 percentile values. Dots represent individual mice. *, $P < 0.05$, by two-tailed t test.

indicate that Iso1/Au/IL12 can exert antitumor effects at much lower doses than those required for IL12. Indeed, a dose of Iso1/Au/IL12 equivalent to 18–19 pg of immunoreactive IL12 (i.e., equivalent to 195–205 pg of bioactive IL12) was sufficient to delay the tumor progression. In contrast, 15 000 pg of bioactive IL12 was necessary to induce similar effects, indicating that Iso1/Au/IL12 was at least 70–80–fold more potent than IL12. Notably, Au/IL12, a nanodrug lacking the isoDGR ligand, could not exert significant effects, supporting the role of isoDGR as a targeting ligand in the antitumor activity of Iso1/Au/IL12. The tumor targeting mechanism is also supported by the observation that low-dose Iso1/Au/IL12 could increase the levels of IFNγ, MIP-2, and sTNF-Rs in tumor tissues, but not in circulation. Importantly, no evidence of toxicity was obtained at any tested dose, indicating that the peptide-tagged nanogold formulation increases the therapeutic index of IL12.

Previous studies showed that a peptide–protein fusion product consisting of IL12 and the vascular-homing peptide CDCRGDCFC, another ligand of $\alpha v\beta 3$ integrin, induced antiangiogenic and antitumor effects when used at 500 000 pg per mouse per day.[8] The observation that 18–19 pg per mouse of Iso1/Au/IL12 was sufficient to induce antitumor effects suggests that Iso1-tagged gold nanoparticles represent more efficient vehicles for delivering IL12 to tumors and for enhancing its therapeutic activity. Other IL12 nanoformulations have been previously described, including nanodrugs prepared with biodegradable poly-lactic acid microspheres,[12b] cholesterol-pullulan nanogel,[12d] chitosan nanoparticles and liposomes.[10,12c] These nanodrugs could induce strong antitumor effects when administered intratumorally,[10,12b] subcutaneously or intravenously at doses ranging from 100 to 10 000 ng per mouse of IL12 in single or repeated administrations,[12c,d] thus at doses well above the efficacious doses of Iso1/Au/IL12 reported in the present work (18–19 pg per mouse). It appears, therefore, that coupling IL12 to the surface of Iso1-tagged gold nanoparticles represents a novel and more potent drug formulation.

Previous studies showed that the dose-response curve of IL12 in patients is bell shaped, with an optimal dose of 250 ng kg^{-1}.[26] We also found a bell-shaped dose-response curve with Iso1/Au/IL12, maximal activity being achieved with 40–80 pg per mouse (equivalent to 2–4 ng of immunoreactive IL12 kg^{-1}). Attempts to increase the effect of Iso1/Au/IL12 by increasing the dose in our models (up to 6000 pg per mouse, i.e., about 300 ng kg^{-1}) or by increasing the frequency of administration (e.g., daily, for 5 consecutive days) resulted in lower antitumor effects. Similar behaviors were reported for other targeted cytokines, such as NGR-TNF and NGR-IFNγ.[27] This paradoxical behavior might be related to antibody induction or, more likely, to activation of counter-regulatory mechanisms. For example, in the case of NGR-TNF and NGR-IFNγ, the use of high doses of these targeted cytokines induces the shedding of soluble TNF receptors or the production of indoleamine-2,3-dioxygenase, respectively, which prevents their potential antitumor activity.[27,28] Activation of counter-regulatory mechanisms likely occurs also with relatively high-dose Iso1/Au/IL12, as suggested by its bell-shaped dose-response curve. Thus, the use of extremely low dose of Iso1/Au/IL12 (in the picogram range) and

nanoparticles with a low number of IL12 molecules could be a strategy for overcoming not only systemic toxic reactions, but also the activation of systemic counter-regulatory effects.

The results of mechanistic studies show that Iso1/Au/IL12 can therapeutically reprogram proinflammatory and antitumor functions in the tumor microenvironment, by increasing tumor infiltration by innate immune cells, such as NK cells, monocytes, and neutrophils. Considering that IL12 was originally described as an NK-stimulating factor,[29] it is not surprising that IL12 targeted to the tumor could act on innate immunity.[30] What is most surprising is that this effect was achieved with an extremely low dose (18 pg) of nanodrug. Iso1/Au/IL12 also recruited intratumorally a small $CD3^+$ population that was identified as invariant natural killer T (iNKT) cells, which is a peculiar subset of T lymphocytes characterized by the expression of a conserved, invariant T cell receptor α chain (TCR Va14-Ja18 in mice, Va24-Ja18 in humans). iNKT cells respond to IL12 and modulate innate effectors in the tumor microenvironment.[31] As iNKT cells are known to be major drivers of the IL12-mediated antitumor effects,[32] it is reasonable to hypothesize that their recruitment to the tumor microenvironment may help activating NK cells and M1 macrophages.[21] This view is supported by the observation that an NK cell-depleting antibody could completely inhibit the antitumor activity of Iso1/Au/IL12 in the WEHI-164 fibrosarcoma model.

Finally, we also found that low-dose Iso1/Au/IL12 could enhance the efficacy to adoptive T cell therapy in mice with autochthonous prostate cancer. In these mice, T cells redirected to the tumor by a TCR gene transfer approach fail to evoke tumor rejection, unless combined with additional tumor-targeting strategies.[24,33] Our results show that adoptive T-cell therapy in combination with low-dose Iso1/Au/IL12 promotes tumor regression in the majority of mice. In previous studies, synergistic activity has been observed also with tumor-specific T cells engineered to express IL12 constitutively or under the control of TCR-regulated (NFAT-IL12) expression.[15b-e,34] Despite improved antitumor effects and limited toxicity was observed in mice with this strategy,[15e] unacceptable toxicity was reported in melanoma patients.[35] More recently, a Tet-regulated IL12 expression system, via doxycycline, was developed.[15f] Interestingly, the transient induction of IL12 in the first days after adoptive T-cell therapy could reprogram the tumor microenvironment, boost the number of tumor-infiltrating T cells with reduced expression of PD1, and improve tumor response.[15f] The stroma remodeling observed in our models after Iso1/Au/IL12 administration might contribute to the antitumor response in the context of adoptive T-cell therapy, resulting in higher frequencies of tumor-specific T cells with effector function and tumor rejection. Thus, our targeting strategy appears to recapitulate some of the effects of IL12-engineered T cells, avoiding the risk of overt cytokine production by an expandable population of T cells. Indeed, although Alsaieedi et al. showed that promoting repeated IL12 expression at defined time intervals might be beneficial,[15f] counterregulatory effects and adverse toxic reactions might also develop, for instance upon uncontrollable T cell expansion or T cell recirculation. Administration of defined doses of Iso1/Au/IL12 at appropriate time intervals and exclusively to the tumor could be an alternative approach to maximize antitumor effects and keep toxicity under control. Given that IL12 can also synergize with immune check-point inhibitors,[36] it is also tempting to propose that the therapeutic efficacy of these compounds might benefit of the combination with Iso1/Au/IL12.

An important question that remains to be addressed is how the endothelial-targeted IL12 can affect immune cells. One possible explanation is that when the nanoparticles are delivered to endothelial cells, part of them or of IL12 molecules are released into the tumor microenvironment, thereby reaching immune cells. Iso1/Au/IL12 bound to tumor endothelial cells might also interact with circulating immune cells.

4. Conclusion

We have shown that the preparation of stable and bifunctional gold nanoparticles endowed with both targeting (isoDGR) and effector (IL12) activity is feasible and that extremely low doses of this nanodrug are sufficient to induce antitumor effects, with no evidence of systemic toxicity. Targeted IL12 remodeled the tumor microenvironment promoting NK cell-mediated antitumor effects, and sustained T cell responses in the context of adoptive T-cell therapy, thus promoting complementary antitumor effector responses. The extremely low doses necessary to induce antitumor effects and the favorable toxicological profile of this treatment may open the way to combination studies with other cytokines, immune checkpoint inhibitors, and other immunotherapeutic approaches.

5. Experimental Section

Cell Lines and Reagents: Murine WEHI-164 fibrosarcoma and mammary adenocarcinoma (TS/A) cells were cultured in DMEM supplemented with 10% fetal bovine serum, 2×10^{-3} M glutamine, 50 μg mL^{-1} streptomycin, 100 U mL^{-1} penicillin, and 0.25 μg mL^{-1} amphotericin-B. Human serum albumin (HSA) was from Baxter (Deerfield, IL); bovine serum albumin (BSA) was from Sigma; murine recombinant interleukin-12 (IL12) was from Peprotech; human interleukin-2 was from Novartis; human $\alpha v\beta 3$ was from Immunological Sciences (Rome, Italy). Rabbit antibodies against asialo-GM1, an antigen expressed by NK cells, basophils, monocytes/macrophages, and T cells, were from Biolegend (Poly21460). Cyclic head-to-tail c(CGisoDGRG) peptide (called Iso1) was prepared and characterized as described.[17,19] Iso1-HSA conjugate, consisting of Iso1 chemically coupled to HSA via 4-(N-maleimidomethyl)cyclohexane-1-carboxylic acid 3-sulfo-N-hydroxysuccinimide ester sodium salt (sulpho-SMCC), was prepared as described.[17,19] For nanodrug preparation, Iso1-HSA and IL12 were dialyzed against 5×10^{-3} M citrate buffer, pH 6.0 and stored at –80 °C.

Preparation of Gold Nanoparticles Functionalized with Iso1-HSA and IL12: Bifunctional gold nanoparticles bearing Iso1-HSA and recombinant IL12 were prepared as follows: 120 μg of Iso1-HSA was mixed with 2.7 μg of IL12 in 100 μL of 5×10^{-3} M sodium citrate buffer, pH 6.0. The mixture was then added to 1 mL of 25 nm gold nanoparticles (Aurion, The Netherlands, with pH adjusted to 4.3–4.4 with orthophosphoric acid) and left to incubate for 1 h at room temperature under shaking (the final pH during the conjugation was ≈5.5). Then, 100 μL of methoxy–PEG–thiol solution (15 μg mL^{-1} in water, M_W 20 KDa, Nanocs) was added to the mixture and left to incubate for 15 min at room temperature. Finally, 100 μL of 10% w/v HSA was added to saturate gold nanoparticles. The mixture was centrifuged and resuspended in 1 mL of 5×10^{-3} M sodium citrate buffer, pH 6.0, containing 1% HSA (three times, 14 000 × g for 15 min). The final product (1 mL) was filtered

(0.22 μm) and stored at –80 °C. Monofunctional nanodrugs lacking Iso1 (bearing IL12 and HSA activated with sulfo-SMCC and quenched with β-mercaptoethanol) were also prepared as described above. This product was called Au/IL12.

Characterization of the Functional and Physicochemical Properties of Nanodrugs: Visible spectra of nanoparticles (Nps) were recorded using an UltroSpec 2100 spectrophotometer (Amersham Biosciences) using 1 cm path-length quartz cuvette. Nanoparticle (Np) concentration was calculated by interpolation on a calibration curve obtained with various solution of uncoated gold in 5×10^{-3} M sodium citrate buffer, pH 6.0 (stock solution: 3.3×10^{11} Nps mL^{-1}, A530 nm ≈0.96 U mL^{-1}).

Dynamic light scattering (DLS) measurements were performed using a DLS DYNAPRO 99 instrument (Wyatt) operating with the laser intensity set to 20% of power. Gold Nps were diluted 1:10 in 5×10^{-3} M sodium citrate buffer, pH 6.0 (1–3 $\times 10^{10}$ Nps mL^{-1}) and analyzed with 25–30 independent measurements of 10 s duration, at 20 °C. The calculation of the hydrodynamic radius of the nanoparticles was performed by DLS regularization analysis.

Z-potential measurements were performed using a ZetaSizer Nano ZS instrument (Malver) equipped with the Zetasizer software (version 7.12). Gold Nps were diluted 1:10 in 5×10^{-3} M sodium citrate buffer, pH 6.0, containing 10 mg mL^{-1} HSA (1–3 $\times 10^{10}$ Nps mL^{-1}) and analyzed with three independent measurements at 25 °C.

IL12- and PEG-ELISA: The amount of total IL12 bound to nanoparticles was quantified by sandwich IL12-ELISA using an in-house protocol as described in Supporting Information and the MAX Deluxe Set Mouse IL12 (p70) ELISA kit (Biolegend).

The amount of mPEG-SH bound to nanoparticle was quantified by competitive-ELISA using a commercial kit (Polyethylene Glycol Backbone ELISA-Kit, Life Diagnostics, Inc), according to the manufacturer's instructions (see Supporting Information). mPEG-SH 20 KDa was used as a reference standard.

αvβ3 Integrin and Anti-IL12 Antibody Sandwich Assays: The binding assays of nanodrug to αvβ3 integrin and to anti-IL12 antibodies spotted onto nitrocellulose filters were performed essentially as described.[17,19] A soluble TNF receptor type-2 fusion protein (sTNF-R2, ENBREL) was used as a negative control.

The αvβ3-integrin/anti-IL12-antibody sandwich assay of nanodrugs was performed as described in Supporting Information.

IL12 Bioassay: The amount of bioactive IL12 bound to gold nanoparticles was determined using an in vitro bioassay based on the capability of IL12 to induce the release of interferon-γ (IFNγ) from murine splenocytes as described in Supporting Information.

In Vivo studies: Studies in animal models were approved by the Ethical Committee of the San Raffaele Scientific Institute and performed according to the prescribed guidelines.

Subcutaneous Tumors: BALB/c or C57BL/6N mice (Charles River Laboratories), weighing 16 to 18 g, were challenged with subcutaneous injection in the left flank of 1.5×10^6 WEHI-164 or 3×10^5 TS/A living cells. Tumor-bearing mice were randomized and assigned to various experimental groups in order to obtain groups with similar average tumor size before treatment. Mice were injected, i.v., with nanodrugs in 0.9% sodium chloride solution (Laboratorio Farmacologico SALF, Bergamo, Italy) containing 100 μg mL^{-1} of HSA. Tumor growth was monitored by measuring tumor size with calipers. The tumor volume was estimated by calculating $r1 \times r2 \times r3 \times 4/3\pi$, where $r1$ and $r2$ are the longitudinal and lateral radii, and $r3$ is the thickness of the tumor protruding from the surface of normal skin. Animals were sacrificed before tumors reached a diameter of 1.0 to 1.5 cm. Tumor sizes are shown as mean±SE.

Autochthonous Prostate Cancer Model: Heterozygous CD45.2$^+$ C57BL/6 TRAMP mice and wild-type CD45.1$^+$ congenic mice, were housed, bred, and genotyped in a specific pathogen-free animal facility in accordance with the European Union guidelines.[33,37] Congenic CD45.1$^+$ cells were transduced with a tumor (Tag-IV)-specific TCR as previously described.[24,33] Twenty- week-old male TRAMP mice were conditioned by a sublethal dose of total body irradiation (6 Gy), and the following day i.v. injected with transduced cells containing 0.5×10^6 TCR redirected CD8$^+$ T cells. The next day, the animals were injected (i.v.) with Iso1/Au/L12 (18 pg, in saline solution containing 100 μg mL^{-1} of HSA) or with diluent. At day 28, urogenital apparata (UGA) were processed for histology and prostate tissues were scored by a dedicated pathologist, as previously described with some modification.[24,33] Briefly, complete regression (100%), defined as area without evidence of residual diseases; partial regression (25–75%) defined as area of complete regression scattered among acini affected by adenocarcinoma; no regression (0%). Mice bearing highly aggressive poorly differentiated neuroendocrine tumors were excluded from the study.

Quantification of Soluble TNF-Receptor 2, IFNγ and MIP-2 into the Tumor Mass: Soluble TNF-receptor 2, IFNγ and MIP-2 were detected by ELISA as described in Supporting Information.

Flow Cytometry Analysis: WEHI-164 tumor-bearing mice were treated at day 6 after tumor implantation with Iso1/Au/IL12 (18 pg) or diluent. At day 13, tumors were removed, weighted, minced in small pieces and resuspended with the mouse Tumor Dissociation Kit (2.5 mL g^{-1}, Miltenyi Biotec GmbH), according to the manufacturer's instruction. Minced tissues were then automatically processed with the gentleMACS Octo Dissociator (using preloaded program m_TDK_02, Miltenyi) to obtain a single cell suspension. After dissociation, the cell suspension was filtered through a 30 μm filter. Cell staining was performed as follows: 10^7 cells were washed twice with "*FACS buffer*" (PBS containing 2% FBS and 0.2% sodium azide) and incubated for 15 min with FACS buffer containing normal mouse IgG (150 μg mL^{-1}, Jackson ImmunoResearch) at 4 °C. After washing, the cells were resuspended in PBS containing Live/Dead Blue reagent (Invitrogen, 0.1 μL per 50 μL sample) and left to incubate for 30 min at room temperature. After washing with FACS buffer, the cells were incubated for 30 min with PBS-57-loaded CD1d tetramer (0.75 μg per 50 μL in FACS buffer), washed again and incubated with mixture of fluorochrome-conjugated monoclonal antibodies (Table S1, Supporting Information, 50 μL per sample) in Brilliant Staining Buffer (BD Horizon) (20 min on ice). After two additional washings the cells were analyzed using a flow cytometer (BD LRSFortessa) (5×10^4 events gated on CD45$^+$ and live cells) and the FlowJo software for compensation and quality before the high dimensional analysis.

In the case of TRAMP mice, peripheral blood, tumor draining popliteal lymph nodes (TdLN) and spleen were collected. Single-cell suspensions were generated and analyzed immediately or were stimulated with 2×10^{-3} M Tag-IV peptide (VVYDFLKC) for 4 h of which the last 2 h were in the presence of Brefeldin A. Cells were surface stained, fixed, and permeabilized, and further stained for intracellular IFNγ as described previously.[24,33] IFNγ production in the absence of stimulation was considered as background release and subtracted from values obtained in response to specific peptides. Intracellular Granzyme B levels were analyzed immediately after organ explant. Dead cells were labeled with 7AAD and samples were acquired on a BD FACSCanto II cell analyzer. Doublets were distinguished and excluded by plotting FSC area versus FSC height and data analysis was performed using FlowJo software.

High Dimensional Flow Cytometry Data Analysis: Primary FCS data were exported from FlowJo after gating on lymphocytes, singlets and viable CD45+ cells and were fed into the X-Shift algorithm, which automatically detects the best number of clusters (i.e., cell populations) with diverse phenotype in the whole dataset.[22] Simultaneously, the t-Distribution Stochastic Neighbor Embedding algorithm (viSNE[21,38]) was employed to build 2D maps on the basis of the expression level of each single marker included in the staining. FCS files including bhSNE maps and X-Shift clustering were then exported and analyzed in FlowJo to evaluate the cluster frequency and marker signature in single samples.

Statistics: Statistical analysis was performed using the Prism software (version 8, GraphPad). Data distribution was assessed using the D'Agostino and Pearson omnibus normality test. Unpaired *t* test (two-tailed) and Mann-Whitney tests were used for normally and nonnormally distributed data, respectively. Differences were considered significant with a *P* value lower than 0.05.

Supporting Information

Supporting Information is available from the Wiley Online Library or from the author.

Acknowledgements

A.M.G. and A.S. contributed equally to this work. The authors thank Dr. Maria Carla Panzeri of the Advanced Light and Electron Microscopy BioImaging Center (ALEMBIC, San Raffaele Scientific Institute) for TEM analysis. This work was supported by grants from Ministero della Salute of Italy (RF-2011-02350836 to AC, and RF-2016-02361054 to FC) and Associazione Italiana Ricerca sul Cancro (AIRC IG19220 and Id. 22737 to AC, and IG15883 to AM). The authors are grateful to NIH Tetramer Core Facility for providing the mouse CD1d tetramers.

Conflict of Interest

F.C and A.C are inventors of patents regarding the use of Iso1/Au/IL12. The other authors have declared that no conflict of interest exists.

Keywords

gold nanoparticles, immunotherapy, interleukin-12, isoDGR motif, $\alpha v\beta 3$ integrin

Received: July 2, 2019
Revised: August 26, 2019
Published online:

[1] a) M. J. Brunda, L. Luistro, R. R. Warrier, R. B. Wright, B. R. Hubbard, M. Murphy, S. F. Wolf, M. K. Gately, *J. Exp. Med.* **1993**, *178*, 1223; b) B. A. Teicher, G. Ara, K. Menon, R. G. Schaub, *Int. J. Cancer* **1996**, *65*, 80; c) K. Kozar, R. Kaminski, T. Switaj, T. Oldak, E. Machaj, P. J. Wysocki, A. Mackiewicz, W. Lasek, M. Jakobisiak, J. Golab, *Clin. Cancer Res.* **2003**, *9*, 3124; d) B. A. Teicher, G. Ara, D. Buxton, J. Leonard, R. G. Schaub, *Clin. Cancer Res.* **1997**, *3*, 1661; e) W. Lasek, R. Zagozdzon, M. Jakobisiak, *Cancer Immunol. Immunother.* **2014**, *63*, 419; f) S. Tugues, S. H. Burkhard, I. Ohs, M. Vrohlings, K. Nussbaum, J. Vom Berg, P. Kulig, B. Becher, *Cell Death Differ.* **2015**, *22*, 237; g) J. M. Weiss, J. J. Subleski, J. M. Wigginton, R. H. Wiltrout, *Expert Opin. Biol. Ther.* **2007**, *7*, 1705.

[2] M. Aste-Amezaga, A. D'Andrea, M. Kubin, G. Trinchieri, *Cell. Immunol.* **1994**, *156*, 480.

[3] C. S. Hsieh, S. E. Macatonia, C. S. Tripp, S. F. Wolf, A. O'Garra, K. M. Murphy, *Science* **1993**, *260*, 547.

[4] a) C. M. van Herpen, R. van der Voort, J. A. van der Laak, I. S. Klasen, A. O. de Graaf, L. C. van Kempen, I. J. de Vries, T. D. Boer, H. Dolstra, R. Torensma, J. H. van Krieken, G. J. Adema, P. H. De Mulder, *Int. J. Cancer* **2008**, *123*, 2354; b) G. Trinchieri, *Annu. Rev. Immunol.* **1995**, *13*, 251.

[5] P. Berraondo, I. Etxeberria, M. Ponz-Sarvise, I. Melero, *Clin. Cancer Res.* **2018**, *24*, 2716.

[6] U. Grohmann, M. L. Belladonna, R. Bianchi, C. Orabona, E. Ayroldi, M. C. Fioretti, P. Puccetti, *Immunity* **1998**, *9*, 315.

[7] a) S. Jenks, *J. Natl. Cancer Inst.* **1996**, *88*, 576; b) J. P. Leonard, M. L. Sherman, G. L. Fisher, L. J. Buchanan, G. Larsen, M. B. Atkins, J. A. Sosman, J. P. Dutcher, N. J. Vogelzang, J. L. Ryan, *Blood* **1997**, *90*, 2541; c) M. Del Vecchio, E. Bajetta, S. Canova, M. T. Lotze, A. Wesa, G. Parmiani, A. Anichini, *Clin. Cancer Res.* **2007**, *13*, 4677.

[8] E. B. Dickerson, N. Akhtar, H. Steinberg, Z. Y. Wang, M. J. Lindstrom, M. L. Padilla, R. Auerbach, S. C. Helfand, *Mol. Cancer Res.* **2004**, *2*, 663.

[9] a) L. S. Peng, M. L. Penichet, S. L. Morrison, *J. Immunol.* **1999**, *163*, 250; b) C. Halin, S. Rondini, F. Nilsson, A. Berndt, H. Kosmehl, L. Zardi, D. Neri, *Nat. Biotechnol.* **2002**, *20*, 264; c) J. Li, P. Hu, L. A. Khawli, A. Yun, A. L. Epstein, *Hybridoma Hybridomics* **2004**, *23*, 1; d) J. Fallon, R. Tighe, G. Kradjian, W. Guzman, A. Bernhardt, B. Neuteboom, Y. Lan, H. Sabzevari, J. Schlom, J. W. Greiner, *Oncotarget* **2014**, *5*, 1869.

[10] M. R. Simpson-Abelson, V. S. Purohit, W. M. Pang, V. Iyer, K. Odunsi, T. L. Demmy, S. J. Yokota, J. L. Loyall, R. J. Kelleher Jr., S. Balu-Iyer, R. B. Bankert, *Clin. Immunol.* **2009**, *132*, 71.

[11] D. A. Zaharoff, B. S. Hoffman, H. B. Hooper, C. J. Benjamin Jr., K. K. Khurana, K. W. Hance, C. J. Rogers, P. A. Pinto, J. Schlom, J. W. Greiner, *Cancer Res.* **2009**, *69*, 6192.

[12] a) H. C. Hill, T. F. Conway Jr., M. S. Sabel, Y. S. Jong, E. Mathiowitz, R. B. Bankert, N. K. Egilmez, *Cancer Res.* **2002**, *62*, 7254; b) M. S. Sabel, G. Su, K. A. Griffith, A. E. Chang, *Breast Cancer Res. Treat.* **2010**, *122*, 325; c) Q. Xu, L. Guo, X. Gu, B. Zhang, X. Hu, J. Zhang, J. Chen, Y. Wang, C. Chen, B. Gao, Y. Kuang, S. Wang, *Biomaterials* **2012**, *33*, 3909; d) T. Shimizu, T. Kishida, U. Hasegawa, Y. Ueda, J. Imanishi, H. Yamagishi, K. Akiyoshi, E. Otsuji, O. Mazda, *Biochem. Biophys. Res. Commun.* **2008**, *367*, 330.

[13] a) C. Xu, Y. Zhang, P. A. Rolfe, V. M. Hernandez, W. Guzman, G. Kradjian, B. Marelli, G. Qin, J. Qi, H. Wang, H. Yu, R. Tighe, K. M. Lo, J. M. English, L. Radvanyi, Y. Lan, *Clin. Cancer Res.* **2017**, *23*, 5869; b) J. K. Fallon, A. J. Vandeveer, J. Schlom, J. W. Greiner, *Oncotarget* **2017**, *8*, 20558; c) J. Strauss, C. R. Heery, J. W. Kim, C. Jochems, R. N. Donahue, A. S. Montgomery, S. McMahon, E. Lamping, J. L. Marte, R. A. Madan, M. Bilusic, M. R. Silver, E. Bertotti, J. Schlom, J. L. Gulley, *Clin. Cancer Res.* **2019**, *25*, 99.

[14] A. I. Daud, R. C. DeConti, S. Andrews, P. Urbas, A. I. Riker, V. K. Sondak, P. N. Munster, D. M. Sullivan, K. E. Ugen, J. L. Messina, R. Heller, *J. Clin. Oncol.* **2008**, *26*, 5896.

[15] a) J. I. Quetglas, S. Labiano, M. A. Aznar, E. Bolanos, A. Azpilikueta, I. Rodriguez, E. Casales, A. R. Sanchez-Paulete, V. Segura, C. Smerdou, I. Melero, *Cancer Immunol. Res.* **2015**, *3*, 449; b) L. Zhang, S. P. Kerkar, Z. Yu, Z. Zheng, S. Yang, N. P. Restifo, S. A. Rosenberg, R. A. Morgan, *Mol. Ther.* **2011**, *19*, 751; c) M. Chmielewski, C. Kopecky, A. A. Hombach, H. Abken, *Cancer Res.* **2011**, *71*, 5697; d) M. Chmielewski, H. Abken, *Cell Rep.* **2017**, *21*, 3205; e) A. Kunert, M. Chmielewski, R. Wijers, C. Berrevoets, H. Abken, R. Debets, *OncoImmunology* **2018**, *7*, e1378842; f) A. Alsaieedi, A. Holler, P. Velica, G. Bendle, H. J. Stauss, *OncoImmunology* **2019**, *8*, 1542917.

[16] a) F. Curnis, R. Longhi, L. Crippa, A. Cattaneo, E. Dondossola, A. Bachi, A. Corti, *J. Biol. Chem.* **2006**, *281*, 36466; b) F. Curnis, A. Sacchi, A. Gasparri, R. Longhi, A. Bachi, C. Doglioni, C. Bordignon, C. Traversari, G. P. Rizzardi, A. Corti, *Cancer Res.* **2008**, *68*, 7073; c) A. Spitaleri, S. Mari, F. Curnis, C. Traversari, R. Longhi, C. Bordignon, A. Corti, G. P. Rizzardi, G. Musco, *J. Biol. Chem.* **2008**, *283*, 19757; d) A. Spitaleri, M. Ghitti, S. Mari, L. Alberici, C. Traversari, G. P. Rizzardi, G. Musco, *Angew. Chem., Int. Ed.* **2011**, *50*, 1832; e) J. S. Desgrosellier, D. A. Cheresh, *Nat. Rev. Cancer* **2010**, *10*, 9; f) C. J. Avraamides, B. Garmy-Susini, J. A. Varner, *Nat. Rev. Cancer* **2008**, *8*, 604; g) K. Chen, X. Chen, *Theranostics* **2011**, *1*, 189; h) H. Jin, J. Varner, *Br. J. Cancer* **2004**, *90*, 561.

[17] F. Curnis, A. Sacchi, R. Longhi, B. Colombo, A. Gasparri, A. Corti, *Small* **2013**, *9*, 673.

[18] A. Corti, A. M. Gasparri, M. Ghitti, A. Sacchi, F. Sudati, M. Fiocchi, V. Buttiglione, L. Perani, A. Gori, S. Valtorta, R. M. Moresco, F. Pastorino, M. Ponzoni, G. Musco, F. Curnis, *Adv. Funct. Mater.* **2017**, *27*, 1701245.

[19] F. Curnis, M. Fiocchi, A. Sacchi, A. Gori, A. Gasparri, A. Corti, *Nano Res.* **2016**, *9*, 1393.

[20] F. N. Lauw, P. E. Dekkers, A. A. te Velde, P. Speelman, M. Levi, M. Kurimoto, C. E. Hack, S. J. van Deventer, T. van der Poll, *J. Infect. Dis.* **1999**, *179*, 646.

[21] F. Cortesi, G. Delfanti, A. Grilli, A. Calcinotto, F. Gorini, F. Pucci, R. Luciano, M. Grioni, A. Recchia, F. Benigni, A. Briganti,

A. Salonia, M. De Palma, S. Bicciato, C. Doglioni, M. Bellone, G. Casorati, P. Dellabona, *Cell Rep.* **2018**, *22*, 3006.

[22] a) N. Samusik, Z. Good, M. H. Spitzer, K. L. Davis, G. P. Nolan, *Nat. Methods* **2016**, *13*, 493; b) M. Alcantara-Hernandez, R. Leylek, L. E. Wagar, E. G. Engleman, T. Keler, M. P. Marinkovich, M. M. Davis, G. P. Nolan, J. Idoyaga, *Immunity* **2017**, *47*, 1037.

[23] a) M. Kasai, T. Yoneda, S. Habu, Y. Maruyama, K. Okumura, T. Tokunaga, *Nature* **1981**, *291*, 334; b) I. Kawase, D. L. Urdal, C. G. Brooks, C. S. Henney, *Int. J. Cancer* **1982**, *29*, 567; c) H. Nishikado, K. Mukai, Y. Kawano, Y. Minegishi, H. Karasuyama, *J. Immunol.* **2011**, *186*, 5766.

[24] T. Manzo, T. Sturmheit, V. Basso, E. Petrozziello, R. Hess Michelini, M. Riba, M. Freschi, A. R. Elia, M. Grioni, F. Curnis, M. P. Protti, T. N. Schumacher, R. Debets, M. A. Swartz, A. Corti, M. Bellone, A. Mondino, *Cancer Res.* **2017**, *77*, 658.

[25] S. K. Libutti, G. F. Paciotti, A. A. Byrnes, H. R. Alexander Jr., W. E. Gannon, M. Walker, G. D. Seidel, N. Yuldasheva, L. Tamarkin, *Clin. Cancer Res.* **2010**, *16*, 6139.

[26] a) E. J. Calabrese, L. A. Baldwin, *Annu. Rev. Public Health* **2001**, *22*, 15; b) C. F. Eisenbeis, G. B. Lesinski, M. Anghelina, R. Parihar, D. Valentino, J. Liu, P. Nadella, P. Sundaram, D. C. Young, M. Sznol, M. J. Walker, W. E. Carson 3rd, *J. Clin. Oncol.* **2005**, *23*, 8835.

[27] a) F. Curnis, A. Sacchi, A. Corti, *J. Clin. Invest.* **2002**, *110*, 475; b) F. Curnis, A. Gasparri, A. Sacchi, A. Cattaneo, F. Magni, A. Corti, *Cancer Res.* **2005**, *65*, 2906.

[28] A. M. Gasparri, E. Jachetti, B. Colombo, A. Sacchi, F. Curnis, G. P. Rizzardi, C. Traversari, M. Bellone, A. Corti, *Mol. Cancer Ther.* **2008**, *7*, 3859.

[29] M. Kobayashi, L. Fitz, M. Ryan, R. M. Hewick, S. C. Clark, S. Chan, R. Loudon, F. Sherman, B. Perussia, G. Trinchieri, *J. Exp. Med.* **1989**, *170*, 827.

[30] S. P. Kerkar, R. S. Goldszmid, P. Muranski, D. Chinnasamy, Z. Yu, R. N. Reger, A. J. Leonardi, R. A. Morgan, E. Wang, F. M. Marincola, G. Trinchieri, S. A. Rosenberg, N. P. Restifo, *J. Clin. Invest.* **2011**, *121*, 4746.

[31] a) P. J. Brennan, M. Brigl, M. B. Brenner, *Nat. Rev. Immunol.* **2013**, *13*, 101; b) F. Cortesi, G. Delfanti, G. Casorati, P. Dellabona, *Front. Immunol.* **2018**, *9*, 2375.

[32] J. Cui, T. Shin, T. Kawano, H. Sato, E. Kondo, I. Toura, Y. Kaneko, H. Koseki, M. Kanno, M. Taniguchi, *Science* **1997**, *278*, 1623.

[33] R. Hess Michelini, M. Freschi, T. Manzo, E. Jachetti, E. Degl'Innocenti, M. Grioni, V. Basso, C. Bonini, E. Simpson, A. Mondino, M. Bellone, *Cancer Res.* **2010**, *70*, 3505.

[34] S. P. Kerkar, P. Muranski, A. Kaiser, A. Boni, L. Sanchez-Perez, Z. Yu, D. C. Palmer, R. N. Reger, Z. A. Borman, L. Zhang, R. A. Morgan, L. Gattinoni, S. A. Rosenberg, G. Trinchieri, N. P. Restifo, *Cancer Res.* **2010**, *70*, 6725.

[35] L. Zhang, R. A. Morgan, J. D. Beane, Z. Zheng, M. E. Dudley, S. H. Kassim, A. V. Nahvi, L. T. Ngo, R. M. Sherry, G. Q. Phan, M. S. Hughes, U. S. Kammula, S. A. Feldman, M. A. Toomey, S. P. Kerkar, N. P. Restifo, J. C. Yang, S. A. Rosenberg, *Clin. Cancer Res.* **2015**, *21*, 2278.

[36] a) I. Ohs, L. Ducimetiere, J. Marinho, P. Kulig, B. Becher, S. Tugues, *Cancer Res.* **2017**, *77*, 7059; b) C. S. Garris, S. P. Arlauckas, R. H. Kohler, M. P. Trefny, S. Garren, C. Piot, C. Engblom, C. Pfirschke, M. Siwicki, J. Gungabeesoon, G. J. Freeman, S. E. Warren, S. Ong, E. Browning, C. G. Twitty, R. H. Pierce, M. H. Le, A. P. Algazi, A. I. Daud, S. I. Pai, A. Zippelius, R. Weissleder, M. J. Pittet, *Immunity* **2018**, *49*, 1148.

[37] E. Degl'Innocenti, M. Grioni, A. Boni, A. Camporeale, M. T. Bertilaccio, M. Freschi, A. Monno, C. Arcelloni, N. M. Greenberg, M. Bellone, *Eur. J. Immunol.* **2005**, *35*, 66.

[38] A. D. Amir el, K. L. Davis, M. D. Tadmor, E. F. Simonds, J. H. Levine, S. C. Bendall, D. K. Shenfeld, S. Krishnaswamy, G. P. Nolan, D. Pe'er, *Nat. Biotechnol.* **2013**, *31*, 545.